Atomic structure and magnetic moments in cluster-assembled nanocomposite Fe/Cu films

S. H. Baker,[1] A. M. Asaduzzaman,[1,*] M. Roy,[1] S. J. Gurman,[1] C. Binns,[1] J. A. Blackman,[1,2] and Y. Xie[2]
[1]*Department of Physics and Astronomy, University of Leicester, Leicester LE1 7RH, United Kingdom*
[2]*Department of Physics, University of Reading, Whiteknights, Reading RG6 6AF, United Kingdom*
(Received 8 May 2008; revised manuscript received 9 June 2008; published 22 July 2008)

The atomic structure and net magnetic moments in nanosized Fe clusters embedded in Cu were determined as a function of cluster filling fraction by extended x-ray-absorption fine structure (EXAFS) and magnetometry measurements, respectively. Below the percolation threshold (~25%), the Fe clusters have an fcc structure with a lattice parameter of 3.58 ± 0.02 Å and are ferromagnetic with a net atomic magnetic moment of 0.4–0.9 μ_B. Spin polarized electronic structure calculations were also performed on Fe core/Cu shell systems to investigate the magnetic behavior as a function of lattice spacing; the calculated moments correlate well with experiment.

DOI: 10.1103/PhysRevB.78.014422 PACS number(s): 75.75.+a, 61.46.Df, 61.05.cj

I. INTRODUCTION

Enhancements in the atomic magnetic moments of nanosized clusters of magnetic materials such as Fe or Co, observed in free cluster beams,[1] arise in part due to a significant proportion of atoms with a reduced coordination residing at the surface of the cluster. Subsequent experimental confirmation of enhancements, in both spin and orbital moments, for clusters supported on surfaces[2,3] has led to intensive research efforts to develop "new" high performance magnetic materials assembled from clusters. It is now well established that a flexible way of preparing cluster-assembled materials is to codeposit clusters with an atomic vapor of another material (the matrix material).[4,5] This produces a granular film in which the size and filling fraction of the grains can be varied independently. An additional advantage of this technique is the ability to deposit granular mixtures of miscible materials, for example, granular Fe-Co by depositing Fe nanoclusters in a Co matrix or vice versa.

The atomic structure in embedded nanosized clusters can be strongly influenced by the matrix material. Since some of the key properties, including magnetism, strongly depend on atomic structure it would be advantageous to be able to "engineer" the atomic structure to produce a given set of magnetic properties. For example, the crystal structure of Co clusters embedded in Fe switches from the hcp structure of bulk Co to bcc (Ref. 6); total energy calculations for Co predict a higher magnetic moment in the bcc form than in the normal hcp structure.[7,8]

We report here the measurements of atomic structure and magnetism in nanocomposite Fe/Cu films. The experiments show that embedding Fe clusters in a Cu matrix causes their structure to switch from bcc to fcc, with a sharp change in Fe atomic magnetic moment. The samples were prepared directly by cluster deposition and, unlike in some previous reports[9–12] in which the sizes of fcc Fe granules were as large as 1 μm, the Fe clusters are truly nanosized and single phase.

Using extended x-ray absorption spectroscopy (EXAFS), we have determined that the Fe nanoclusters adopt an fcc structure with a lattice parameter of 3.58 ± 0.02 Å when the volume filling fraction (VFF) of clusters is less than ~25%. Magnetometry measurements show that, in the fcc state, the Fe clusters are ferromagnetic with an average atomic magnetic moment between 0.4 and 0.9 μ_B. We have also performed spin polarized electronic structure calculations to predict magnetic moments for Fe clusters surrounded by outer shells of Cu. The calculations were performed over a range of lattice spacings, and the trends obtained were consistent with the experimental observations.

II. BACKGROUND

It is well known from many theoretical calculations[13–23] on bulk fcc Fe that the magnetization undergoes a transition from a high to a low spin state as the lattice parameter, a, is reduced. The transition occurs fairly sharply in the range 3.4–3.7 Å. Bagayoko and Callaway[15] considered just ferromagnetic solutions. They find that the moment falls steadily to ~2.6 μ_B as the lattice parameter decreases to $a \approx 3.6$ Å; the moments of the bcc and fcc structures are in fact very similar until that point. However below $a \approx 3.6$ Å the fcc moment drops rapidly to zero, while the moment of the bcc structure declines much more slowly with reducing lattice spacing. Other authors find that a transition to an antiferromagnetic phase occurs at roughly the point that Bagayoko and Callaway observed the onset of the rapid decrease in moment in their purely ferromagnetic calculation. Zhou *et al.*[20,21] and Kong[23] reported as many as five different phases at different lattice spacing, but clearly the phases of lowest energy are successively ferromagnetic (FM), antiferromagnetic (AFM), and nonmagnetic (NM) as the lattice parameter is decreased.[16,17,19] The antiferromagnetic phase comprises alternating layers of up and down spins normal to the [001] direction.

The results of our calculations on the bulk material using the tight-binding linear muffin-tin orbital method in the atomic sphere approximation (TB-LMTO-ASA)[24–26] are shown in Fig. 1. The TB-LMTO-ASA scheme is related to the method we use to study clusters. It can be seen from the lower panel that the FM phase is stable for $a \gtrsim 3.62$ Å. Moreover, for smaller values of a, the AFM phase is energetically favored, succeeded at $a \approx 3.48$ Å by a nonmagnetic state. The lattice parameters, at which the transitions occur,

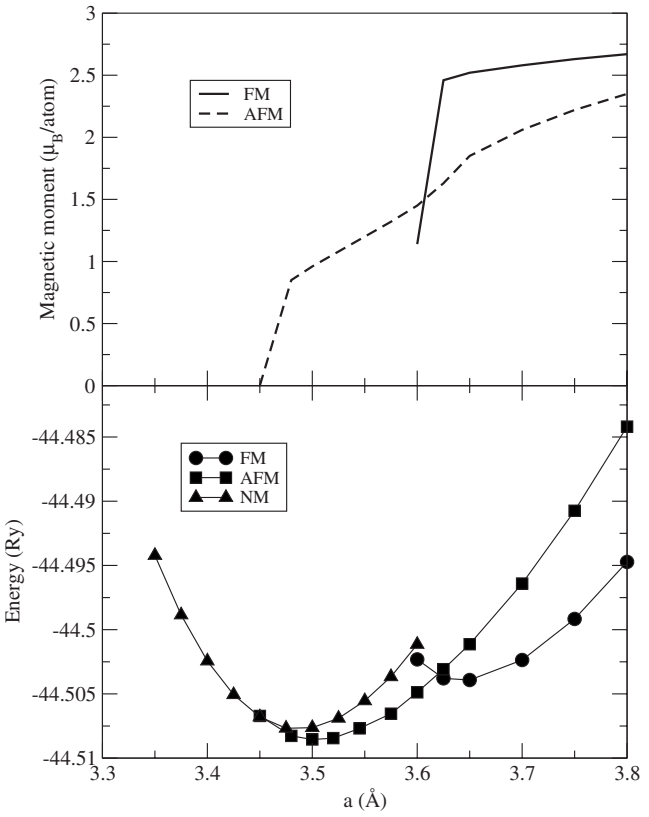

FIG. 1. Lower panel: total energies of bulk fcc Fe as a function of lattice parameter, *a*, showing ferromagnetic (FM), antiferromagnetic (AFM), and nonmagnetic (NM) states. Upper panel: spin magnetic moments of FM and AFM states; note that in the AFM case we show the magnitude of the layer moment per atom.

agree with those found by Moruzzi *et al.*[17] to within 2% despite the fact that their calculations were on fixed moment states and ours were performed with iterations to self-consistency from various trial initial moment configurations. The upper panel in Fig. 1 shows the magnetic moments per atom. The magnitude of the layer magnetization is plotted in the AFM case. The net moment is, of course, zero.

Although fcc γ-Fe can only be stabilized above 1200 K in bulk form, it is now well established experimentally that fcc and fct Fe films can be grown epitaxially at lower temperatures on Cu (Refs. 27–32), which has a small misfit in lattice constant with γ-Fe. Both high moments (>2 μ_B/atom) and low moments (~ 0.5 μ_B/atom) have been reported for fcc/fct Fe films on the (100) (Refs. 29 and 30) and (111) (Refs. 31 and 32) surfaces of Cu. On the (100) surface, high moments are observed for Fe films up to 4 monolayers (ML) (Refs. 29 and 30) although the structure in these films is tetragonally distorted;[28] at higher coverages ($\sim 5-10$ ML), the structure in the films becomes more fcc-like and the moment drops. Fe films grown on Cu(111) have an isotropic fcc structure, with both low moments[31] and high moments[32] reported depending on the deposition method. Gradmann and Isbert[33] deposited thin films of fcc Fe on $Cu_{1-x}Au_x(111)$ surfaces. A low Fe moment ($0.6\mu_B$/atom) was found with a pure Cu substrate, but increasing the Au content expanded the substrate resulting in a switch to a high Fe moment (2.6 μ_B/atom). More recently Torija *et al.*[34] have observed a low spin to high spin thickness driven transition in Fe films on Cu(111) grown at 65 K. The bcc high spin phase develops as the film thickness is increased but the Fe layer at the Fe/Cu interface remains in a low spin state.

In addition to ultrathin films, the fcc structure can also be seen in Fe precipitates in Cu (Refs. 9–11). Neutron-diffraction experiments on single crystals of CuFe alloy containing a few atomic percent Fe, where the diameter of the fcc Fe precipitates was 1 μm, showed antiferromagnetic behavior with atomic moments per Fe atom of ~ 0.7 μ_B (Refs. 9 and 10). Later measurements on similar samples, with diameters of the fcc Fe precipitates in the range of 10s–100s nm, also revealed antiferromagnetic behavior with higher Néel temperatures for larger precipitates.[11] It has also been reported that fcc Fe particles with a mean diameter of 8 nm can be deposited by laser-induced dielectric breakdown of $Fe(CO)_5$ and that they are paramagnetic down to a temperature of 1.8 K, although there is a mixture of bcc and fcc as well as oxide phases present.[12]

Finally we should mention the current interest in Fe/Cu alloys, which (despite their low miscibility) can be prepared over most of the compositional range by mechanical alloying.[35] Magnetization,[35,36] neutron-scattering,[36] and XMCD measurements[37] and theoretical calculations[23,38] have been performed to correlate the variation in magnetism with structure across the composition range. At intermediate concentrations (about 20%–70% Fe), the alloy forms an fcc phase and shows a very small thermal expansion below the magnetic ordering temperature, i.e., it displays an Invar effect. A high Fe moment ($1.5-2$ μ_B/atom) is observed because the presence of the Cu expands the lattice in comparison with that of pure fcc Fe. However it should be noted that the Fe/Cu solid solution is metastable, and high temperatures induce segregation.[36]

III. EXPERIMENT RESULTS

The nanocomposite Fe/Cu films in this study were prepared by codeposition using an ultrahigh vacuum compatible gas aggregation source, described in detail elsewhere,[39] and a Cu molecular beam epitaxy (MBE) source. The sizes of clusters produced in the source follow a logarithmic-normal distribution, with a most probable size of ~ 260 atoms/cluster corresponding to ~ 2 nm diameter. Samples for EXAFS and magnetometry experiments were deposited onto Si(100) and PEEK (poly-ether-ether-ketone) substrates, respectively. For the purposes of comparison, a 500 Å film of Fe was also grown using an MBE source. In all cases, 150 Å buffer and 400 Å capping layers of Ag were deposited *in situ* (from an MBE source) in order to protect the samples against oxidation after removal from the deposition chamber.

A. EXAFS measurements

As demonstrated elsewhere,[6] the element specific and local nature of EXAFS makes it well suited to probing structure in nanocomposite materials. Fe K edge EXAFS experiments were performed on beamline 7.1 of the Synchrotron

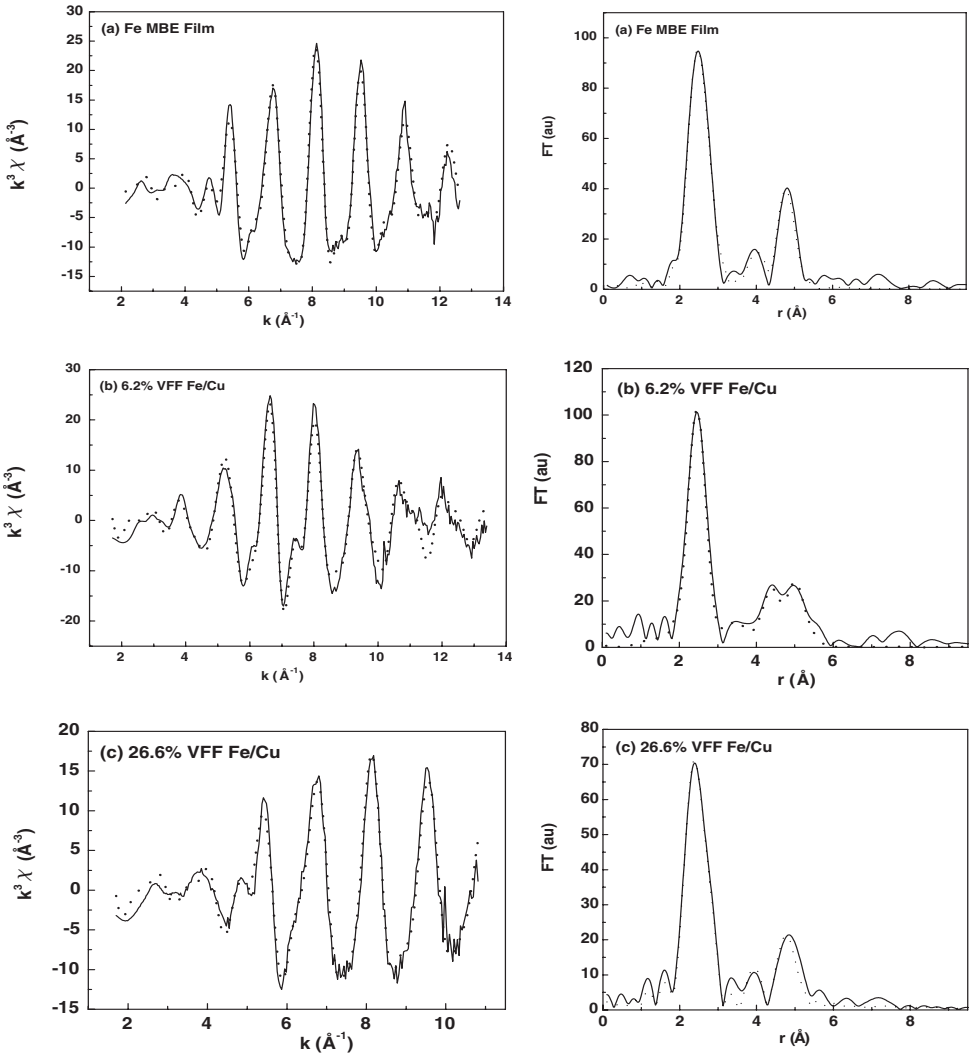

FIG. 2. Fe K edge EXAFS, weighted by k^3, and associated Fourier transform for (a) thick Fe MBE film, (b) 6.2% VFF Fe cluster/Cu film, and (c) 26.6% VFF Fe cluster/Cu film. The full lines represent the data and the dashed lines represent the fits.

Radiation Source at Daresbury Laboratory. The Fe edge absorption spectra $\mu(E)$ were measured in fluorescence using a nine-element monolithic Ge detector and a double crystal Si(111) monochromator, with the incident x-ray intensity measured using an ionization chamber containing an Ar/He gas mixture. The measured absorption spectra $\mu(E)$ were background-subtracted and normalized to yield the EXAFS spectra $\chi(E)$. These could then be analyzed to obtain experimental values for structural parameters such as interatomic distances r_i, mean square variations in interatomic distances σ_i^2 (Debye-Waller factor), and coordination numbers N_i by fitting the experimental $\chi(E)$ to calculated EXAFS functions. This was achieved with the program EXCURV98 (Ref. 40), as described in more detail elsewhere.[6]

Figure 2(a) shows the EXAFS χ (weighted by k^3) and associated Fourier transform for the thick MBE-grown Fe film, where k is the photoelectron wave vector. A good fit to the data was obtained, with four statistically significant shells; the fit was consistent with the bcc structure, as expected for bulk Fe at room temperature. In the fitting procedure, N_i were held fixed at bcc values while r_i and σ_i^2 were allowed to vary freely. The fitted values for r_i and σ_i^2 are listed in Table I, along with those for bulk bcc Fe. The k^3-weighted EXAFS and Fourier transform for a nanocomposite Fe/Cu sample containing 6.2% VFF Fe clusters in Cu are shown in Fig. 2(b). Comparison with those for the bcc Fe film reveals qualitative differences. This is reinforced by the data analysis, which gives a good four-shell fit consistent with the fcc structure. As in the fit for the thick Fe film, N_i were held fixed but at values associated with the fcc structure. The fit values obtained for r_i and σ_i^2 are given in Table I. The analysis program allows multiple scattering effects to be included; in the fit here, we allowed for multiple scattering between the first and fourth shells, as expected in fcc structures. Also included in Table I are r_i and N_i for bulk γ-Fe. The figure of 2.53 Å for the nearest-neighbor distance r_1 in the 6.2% VFF Fe/Cu film implies that the lattice parameter a_0 in the fcc Fe clusters is 3.58 ± 0.02 Å; this is close to the values of a_0 in γ-Fe and Cu, 3.59 Å and 3.61 Å, respectively. Values for r_i and σ_i^2 obtained from fitting the EXAFS for the other nanocomposite Fe/Cu films are listed in Table I as a function of composition. From 5% VFF, where the Fe clusters are isolated within the Cu matrix, to 25% VFF, where there will be significant agglomerates of clusters within the film, the crystal structure in the Fe clusters remains fcc. At higher cluster filling fractions, the atomic structure rapidly switches to bcc, consistent with a three-dimensional percolation threshold of 24.88%.[41] Figure 2(c)

TABLE I. Structural parameters r_i and σ_i^2 obtained from fits to Fe K edge EXAFS for nanocomposite Fe/Cu films.

	Structure	Shell 1	Shell 2	Shell 3	Shell 4
Bulk Fe	bcc	$r_1=2.49$ Å, $N_1=8$	$r_2=2.87$ Å, $N_2=6$	$r_3=4.06$ Å, $N_3=12$	$r_4=4.76$ Å, $N_4=24$
γ-Fe	fcc	$r_1=2.54$ Å, $N_1=12$	$r_2=3.59$ Å, $N_2=6$	$r_3=4.40$ Å, $N_3=24$	$r_4=5.08$ Å, $N_4=12$
Fe MBE	bcc	$r_1=2.49\pm0.01$ Å $2\sigma_1^2=0.011\pm0.001$ Å^2	$r_2=2.86\pm0.02$ Å $2\sigma_2^2=0.020\pm0.003$ Å^2	$r_3=4.12\pm0.02$ Å $2\sigma_3^2=0.023\pm0.004$ Å^2	$r_4=4.80\pm0.01$ Å $2\sigma_4^2=0.014\pm0.002$ Å^2
5.7% VFF Fe/Cu	fcc	$r_1=2.53\pm0.01$ Å $2\sigma_1^2=0.015\pm0.001$ Å^2	$r_2=3.56\pm0.03$ Å $2\sigma_2^2=0.029\pm0.010$ Å^2	$r_3=4.42\pm0.02$ Å $2\sigma_3^2=0.030\pm0.005$ Å^2	$r_4=5.09\pm0.02$ Å $2\sigma_4^2=0.022\pm0.004$ Å^2
6.2% VFF Fe/Cu	fcc	$r_1=2.53\pm0.01$ Å $2\sigma_1^2=0.015\pm0.001$ Å^2	$r_2=3.55\pm0.03$ Å $2\sigma_2^2=0.026\pm0.008$ Å^2	$r_3=4.43\pm0.02$ Å $2\sigma_3^2=0.027\pm0.004$ Å^2	$r_4=5.08\pm0.02$ Å $2\sigma_4^2=0.021\pm0.003$ Å^2
15.8% VFF Fe/Cu	fcc	$r_1=2.53\pm0.01$ Å $2\sigma_1^2=0.020\pm0.002$ Å^2	$r_2=3.56\pm0.04$ Å $2\sigma_2^2=0.033\pm0.014$ Å^2	$r_3=4.43\pm0.04$ Å $2\sigma_3^2=0.043\pm0.010$ Å^2	$r_4=5.29\pm0.03$ Å $2\sigma_4^2=0.016\pm0.007$ Å^2
25.0% VFF Fe/Cu	fcc	$r_1=2.53\pm0.01$ Å $2\sigma_1^2=0.019\pm0.002$ Å^2	$r_2=3.52\pm0.06$ Å $2\sigma_2^2=0.035\pm0.018$ Å^2	$r_3=4.43\pm0.02$ Å $2\sigma_3^2=0.023\pm0.005$ Å^2	$r_4=5.08\pm0.02$ Å $2\sigma_4^2=0.026\pm0.005$ Å^2
26.6% VFF Fe/Cu	bcc	$r_1=2.49\pm0.01$ Å $2\sigma_1^2=0.012\pm0.001$ Å^2	$r_2=2.84\pm0.03$ Å $2\sigma_2^2=0.036\pm0.008$ Å^2	$r_3=4.11\pm0.03$ Å $2\sigma_3^2=0.031\pm0.008$ Å^2	$r_4=4.78\pm0.02$ Å $2\sigma_4^2=0.022\pm0.004$ Å^2
54.1% VFF Fe/Cu	bcc	$r_1=2.49\pm0.01$ Å $2\sigma_1^2=0.011\pm0.001$ Å^2	$r_2=2.86\pm0.02$ Å $2\sigma_2^2=0.029\pm0.005$ Å^2	$r_3=4.13\pm0.02$ Å $2\sigma_3^2=0.024\pm0.005$ Å^2	$r_4=4.78\pm0.02$ Å $2\sigma_4^2=0.019\pm0.003$ Å^2

shows EXAFS data for a sample with 26.6% VFF of Fe clusters. Qualitative similarities with the data for the bcc Fe film are confirmed in the fit details. As we have noted previously,[6] the Debye-Waller factors tend to increase with increasing shell radius. This can be interpreted as being due to correlations in thermal motions of the near neighbors.[42]

B. Magnetization measurements

Experimental values for the magnetic moments in the embedded Fe clusters were obtained by measuring the saturation magnetization at sample temperatures of 2 and 300 K in an Oxford Instruments vibrating sample magnetometer (VSM). Figure 3 shows the net magnetic moments per atom in the Fe clusters—obtained from magnetometry experiments, plotted as a function of composition. The switch to low moments, between 0.4 and 0.9 μ_B/atom, is very clear as the crystal structure in the Fe clusters changes from bcc to fcc across the percolation threshold. Measurements made at 2 and 300 K yield, within experimental error, the same saturation magnetizations and hence the same moments. This is illustrated in Fig. 4, which shows the magnetization curves at 2 and 300 K for a sample containing 5.4% VFF of (fcc) Fe clusters in Cu. The observations of hysteresis at 2 K shows that the fcc Fe clusters are magnetic at this temperature, although at 300 K they are superparamagnetic. The data indicates that the fcc Fe clusters are not antiferromagnetic, in contrast to earlier reports for larger fcc Fe precipitates in Cu (Refs. 9–11).

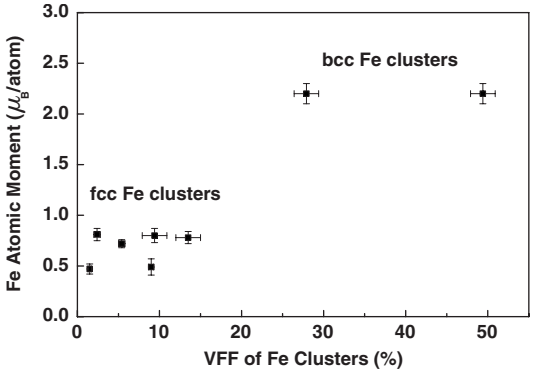

FIG. 3. Magnetic moment per atom in the Fe clusters as a function of composition, as determined from magnetometry experiments.

IV. THEORETIC CALCULATIONS

A. Computational methods

It is not realistic to perform calculations on particles of the size of experimental interest embedded in what is essentially an infinite matrix. Thus our approach is to study Fe core/Cu shell clusters. For simplicity, and because we have no experimental information about the cluster shapes, we confine our calculations to fcc cuboctahedral clusters with O_h symmetry of the form Fe_mCu_{n-m}, where m and n are "magic numbers" for the cuboctahedral system: 55, 147, 309, 561, 923, and $n>m$.

The main interest is at $m=147$ and 309 since these numbers straddle the size studied experimentally. We investigate how the magnetism of the Fe core changes with the number of Cu shells and with the fcc lattice spacing. Most of the calculations are done at fixed lattice spacing and for spin only moments. The contribution from the orbital moment is found to be small. One calculation is done to study the effect of geometry optimization.

We consider here clusters of up to 923 atoms and we use both *ab initio* and tight-binding methodology in the calculations. Our approach is to use tight-binding (TB) methodology for clusters in the size range that is of main interest but, to check the reliability of the TB parametrization, by comparing TB and *ab initio* results on smaller clusters: principally $Fe_{55}Cu_{92}$.

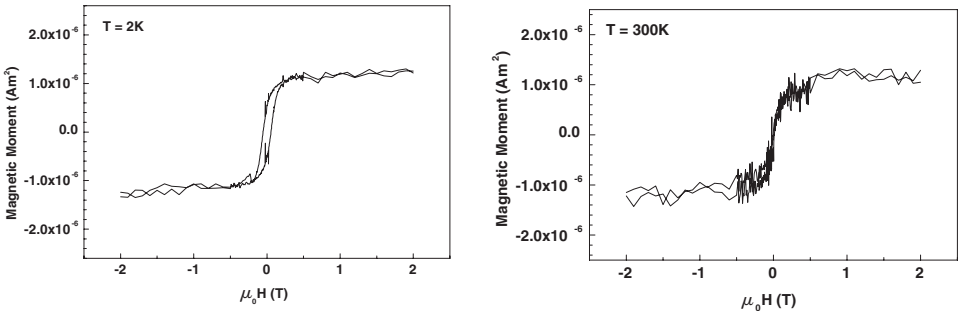

FIG. 4. Magnetization curves for sample containing 5.4% VFF of fcc Fe clusters in Cu.

It is worth noting that, until recently, there have been very few reports of discrete Fourier transform (DFT) calculations on large systems,[43–45] and even fewer reports that are spin-polarized studies. Nava *et al.*[45] consider the effect of spin polarization on a Pd_{140} cluster, for example. Recently, however, calculations have been reported with cluster sizes up to 641 atoms.[46,47]

For the *ab initio* calculations we used the linear combination of atomic orbital (LCAO) method as implemented in the density-functional package DMOL3 (Ref. 48). The atomic orbitals are obtained via a radial solution of the atomic Schrödinger equation. Double numerical basis $3d$ and $4s$ orbitals in addition to $4p$ polarized functions are included in the valence basis set. The core orbitals are allowed to hybridize with the valence orbitals. A generalized gradient approximation, "PW91," (Refs. 49–51) was used to represent the exchange correlation interaction.

TB methodology has been widely used since its early applications to bulk transition metals. In the most commonly used orthogonal form, the TB Hamiltonian is expressed in terms of on-site and nearest-neighbor hopping terms associated with $4s$, $4p$, and $3d$ orbitals, and it can be applied equally to real space or k-space calculations. For spin polarized calculations, on-site exchange parameters are included. The main addition, if the TB method is being applied to clusters (or any system without translational symmetry), is the inclusion of a phenomenological on-site potential to force charge neutrality. A simple functional form for the dependence of the hopping integrals on interatomic distance[52] is often used for calculations with varying geometry.[53] The refinement of TB parameters to improve their transferability from bulk systems to situations in which the atoms are in very different environments has been discussed,[54] including for systems in which more than one element is present.[55,56] However obtaining TB parameters within these schemes is rather laborious.

Fairly recently, a more straightforward way of obtaining TB parameters has been proposed.[57] This is based on the TB-LMTO-ASA method that was used to obtain the moments of bulk fcc Fe in Fig. 1. The essence of the TB-LMTO-ASA method is a transformation between conventional muffin-tin orbitals (MTOs) and tight-binding ones, which is realized through a transformation between bare structure constants S^0 and "screened" structure constants (SSCs) S^α via a Dyson equation,

$$S^\alpha = \alpha^{-1}[(\alpha^{-1} - S^0)^{-1} - \alpha]\alpha^{-1}, \quad (1)$$

where α are site independent screening constants. The SSCs are well localized (they vanish beyond second neighbors) and are material independent (they depend only on the structure). From the SSCs and material dependent potential parameters, one constructs the TB-LMTO-ASA Hamiltonian. Expressions for the ten $(ss\sigma, sp\sigma, pp\sigma, pp\pi, sd\sigma, pd\sigma, pd\pi, dd\sigma, dd\pi, dd\delta)$ bare structure constants, S^0, as a function of interatomic distance was listed by Nowak *et al.*,[26] as are values for the three (s,p,d) screening constants, α.

Our procedure is to obtain the material dependent potential parameters from the bulk calculations and then use them with screened structure constants generated for the clusters using Eq. (1). Thus the parameters of the tight-binding model are obtained directly from *ab initio* calculations within the LMTO-ASA method, without any fitting. In terms of the screened structure constants S^a, the second-order Hamiltonian H in the ASA can be broken down into one, two, and three center terms.

The procedure is described in greater detail in Ref. 57. It was tested[57] for elemental clusters and core-shell systems, and has subsequently been used to study magnetocrystalline anisotropy in Co clusters on Pt (Ref. 58) and, in adapted form, noncollinear magnetism in small Mn clusters.[59] For calculating orbital moments, spin-orbit coupling among the d orbitals in the usual single-site form[60] is added to the tight-binding Hamiltonian and the coupling constants are taken from the last iteration of the self-consistent TB-LMTO-ASA calculations. The tight-binding parameters for the Fe/Cu core-shell clusters were obtained from TB-LMTO-ASA calculations on an ordered binary alloy of Fe and Cu on an fcc lattice with the lattice constant of bulk Cu. We used an Fe_3Cu structure but found essentially the same results if the parameters were derived from the Cu_3Fe structure.

B. Results

The calculations were performed on fcc cuboctahedral Fe clusters containing 55, 147, and 309 atoms. We consider initially bare Fe clusters and then add additional shells of Cu to study the effect of embedding. For most of the calculations, we keep all atoms at fixed positions on the fcc lattice and obtain results over a range of 3.30–3.80 Å lattice spacings.

1. Bare Fe clusters

Figure 5 shows the magnetic moment per atom of 55, 147, and 309 atom Fe clusters as a function of lattice spacing. For some lattice spacings, we found that several metastable solutions could be generated from different starting spin configurations. In these cases, we have presented the lowest-energy solutions in the plots. For a few values of a, we found

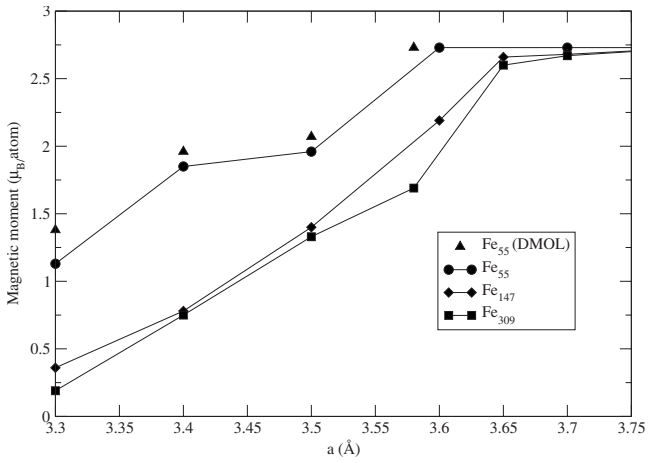

FIG. 5. Calculated spin moment of Fe clusters (55, 147, and 309 atoms) as a function of a (the size of cubic unit cell). Data points joined by lines are from tight-binding calculations. *Ab initio* results for the 55 atom cluster are indicated by filled triangles.

it difficult to get convergence to any stable solution but a slight change in the spacing generally yielded a result. The moment of the 55 atom cluster calculated by DMOL3 is shown by filled triangles. The results for the *ab initio* and the TB calculation are in good agreement with each other, which gives added confidence in our parametrization scheme. We also calculated the moments of the 13 atom cluster (not shown) using the *ab initio* code as a further check and again found good agreement with the results using TB methodology.

It is apparent from Fig. 5 that the moment is reducing with the lowering of the lattice spacing as expected. The moment for $a \gtrsim 3.65$ Å (or 3.60 Å for the 55 atom cluster) changes slowly, but the moment drops off quite fast at smaller lattice spacings, particularly for the larger two clusters. The high moment regime is quite similar in magnitude to that in the bulk calculation of Fig. 1. However it should be emphasized that at the smaller lattice spacings, we are plotting the net moment in Fig. 5, whereas in Fig. 1 it is the magnitude of the atomic moments that are being shown; in the bulk case we are in an antiferromagnetic regime and the net moment is zero.

To get more insight into the magnetic behavior, we have plotted the local moments for the 147 and 309 atom clusters in Figs. 6(a) and 6(b). These sizes straddle that of the clusters of experimental interest (~260 atoms). The results for two lattice parameters are shown: $a=3.70$ Å is in the high moment regime (ferromagnetic in bulk), and at $a=3.50$ Å the moment is reduced to below 1.5 μ_B (antiferromagnetic in bulk). The lattice sites are indicated on the horizontal axis in a notation explained in the figure caption. The calculations produce moment configurations that have O_h symmetry even though this was not imposed by the calculation itself or biased by the initial spin configuration in the iterations to self-consistency. The individual moments at $a=3.70$ Å mostly lie between 2 and 3 μ_B, with some enhancement in the moments on the surface atoms compared to those on the atoms in the core of the cluster. In Fe_{147}, the average moment of the 55 core atoms is 2.0 μ_B, while the 92 surface atoms have a

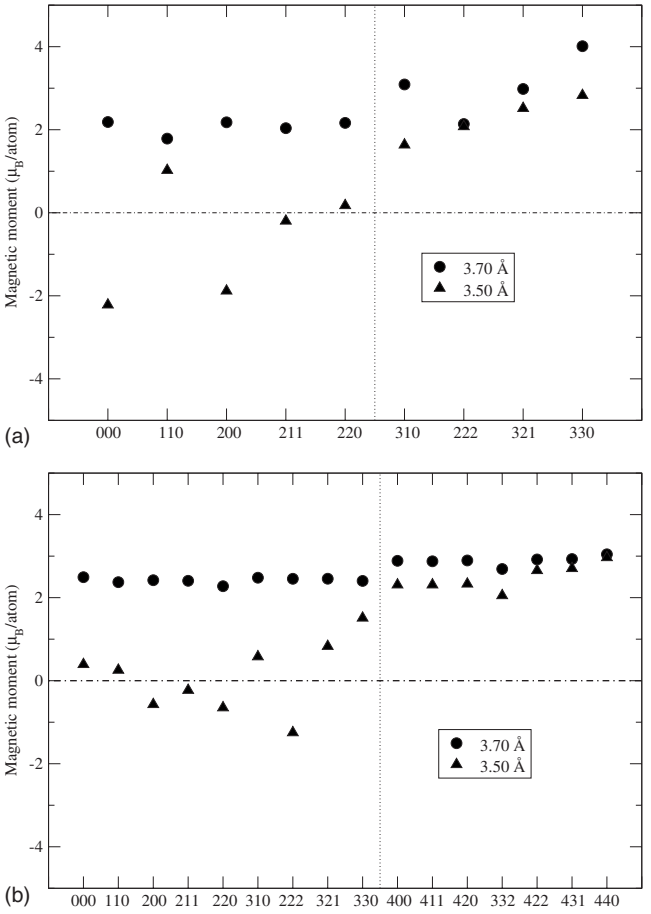

FIG. 6. (a) Spin moment of individual atoms in the 147 atom cluster. The moments are plotted for two lattice spacings: $a=3.70$ Å (circles) and $a=3.50$ Å (triangles). The lattice sites are indicated on the horizontal axis in the conventional notation, i.e., (000) is the central atom of the cluster and the symbols (xyz) are the Cartesian coordinates of the other atoms with respect to the central one in units of half the lattice constant ($a/2$). The moment configuration has O_h symmetry although this was not imposed in the calculation, and so a moment labeled (xyz) refers to an atom at that position and those symmetrically equivalent to it. The vertical dotted line separates the core and surface sites of the cluster. (b) As Fig. 5 for the 309 atom cluster.

mean moment of 3.1 μ_B. The corresponding figures for the 147 atom core and 162 atom surface of Fe_{309} are 2.4 and 2.9 μ_B, respectively.

Turning now to the $a=3.50$ Å lattice spacing, we notice that the surface atoms have their spins aligned ferromagnetically although somewhat reduced in magnitude compared to the $a=3.70$ Å case. However the moments on the core atoms are significantly reduced in magnitude and there is a mixture of positive and negative alignment. Clusters with this lattice spacing then exhibit ferrimagnetism rather than the antiferromagnetism expected in the bulk. The mean core and surface moments are now −0.1 and 2.3 μ_B for Fe_{147}, and 0.3 and 2.5 μ_B for Fe_{309}, respectively. Clearly the surface exerts a strong influence on the behavior and the net moment of the cluster largely comes from the surface contribution. We would envisage that, as we go to larger clusters and the proportion of atoms on the surface decreases, the net ferri-

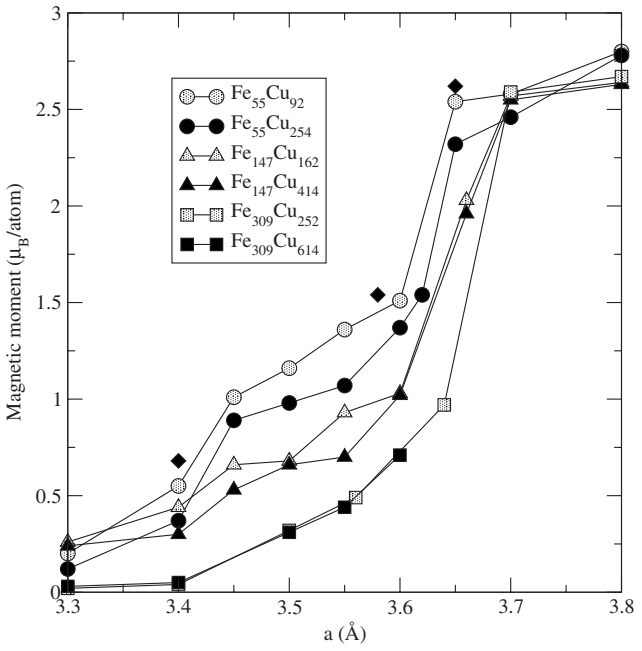

FIG. 7. Calculated spin moment of Fe clusters (55, 147, and 309 atoms), embedded in one of two shells of Cu, as a function of a (the size of cubic unit cell). Data points joined by lines are from tight-binding calculations. *Ab initio* results for the $Fe_{55}Cu_{92}$ cluster are indicated by filled diamonds.

magnet moment will decrease with the eventual convergence to the bulk antiferromagnetic behavior.

2. Fe clusters embedded in Cu shells

We consider now the effect on the magnetic behavior of embedding the Fe clusters in Cu. Results are displayed in Fig. 7 for 55 and 147 atom Fe clusters coated with one and two shells of Cu: $Fe_{55}Cu_{92}$, $Fe_{55}Cu_{254}$, $Fe_{147}Cu_{162}$, $Fe_{147}Cu_{414}$, $Fe_{309}Cu_{252}$, and $Fe_{309}Cu_{614}$. We were unable to obtain convergence to self-consistency for the $Fe_{309}Cu_{614}$ cluster at a few lattice spacings, so there are fewer data points available for this case than for the other clusters. *Ab initio* calculations at representative lattice constants were performed on the smallest cluster $Fe_{55}Cu_{92}$ as a check. The moments obtained are shown in Fig. 7 and again the TB calculations are in good agreement.

Comparing Fig. 7 with the plots shown in Fig. 5, it is seen that the high moment state at large lattice spacings is very little affected by the embedding; the moment remains a little above 2.5 μ_B. However the low moment regime at smaller lattice spacings is much more significantly affected, with all plots in Fig. 7 lying below the Fe_{309} plot in Fig. 5. As with the bare clusters, the moment per atom decreases with increasing cluster size. Comparing the various plots, it appears that a second Cu shell has a decreasing influence on the Fe moment as the size of the cluster increases.

The individual moments for the $Fe_{147}Cu_{162}$ and $Fe_{309}Cu_{252}$ clusters are shown in Figs. 8(a) and 8(b) for the same two lattice parameters $a=3.70$ Å and $a=3.50$ Å, which were used to illustrate the magnetic behavior in bare clusters in Figs. 6(a) and 6(b). Again the calculations produce moment

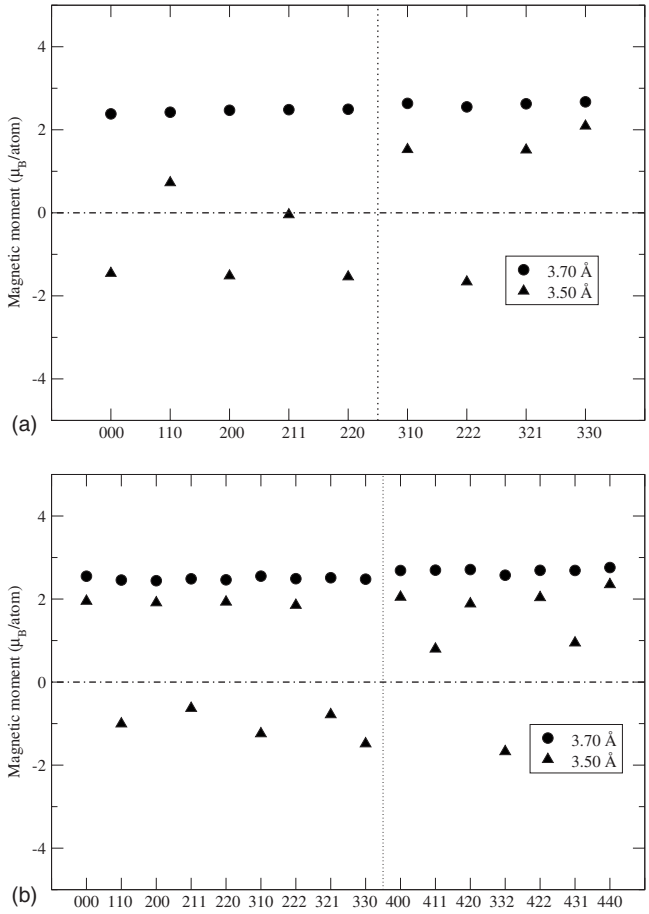

FIG. 8. (a) Spin moment of individual atoms in the 147 atom Fe cluster embedded in a single shell (162 atoms) of Cu. The moments are plotted for two lattice spacings: $a=3.70$ Å (open circle) and $a=3.50$ Å (filled circle). The lattice sites are indicated on the horizontal axis in the same notation as Fig. 5. The moment configuration has O_h symmetry although this was not imposed in the calculation. The vertical dotted line separates the core sites of the Fe cluster from the surface sites, which now interface with the Cu. (b) As Fig. 8 for the 309 atom Fe cluster embedded in a single shell (252 atoms) of Cu.

configurations with O_h symmetry. The surface atoms of the Fe clusters are now at the interface with the Cu and so their coordination number is restored to 12. Despite this, for the large lattice spacing ($a=3.70$ Å), the embedding in Cu results in rather little change in the moments from their bare cluster behavior, with individual moments mostly still lying in the 2–3 μ_B range. The surface atoms in the bare Fe clusters are now at the interface with the Cu. The average core and interface moments are 2.5 and 2.6 μ_B for $Fe_{147}Cu_{162}$, and 2.5 and 2.7 μ_B for $Fe_{309}Cu_{252}$, respectively. Comparing these figures with the bare cluster case, it is seen that the main effect of the embedding is to bring the core and surface/interface moments closer in value (see Table II).

The behavior in the low moment state (at $a=3.50$ Å differs somewhat from that in the bare cluster. A number of the outer Fe atoms, which are now at the interface with the Cu shell, have reduced moments and, in both the 147 and the 309 atom clusters, one atom (and those symmetrically

TABLE II. Mean spin moments of core and surface (or interface) atoms for bare and embedded Fe clusters at two lattice spacings.

	$a=3.50$ Å		$a=3.70$ Å	
	core (μ_B)	surf (μ_B)	core (μ_B)	surf (μ_B)
Fe_{147}	−0.1	2.3	2.1	3.1
$Fe_{147}Cu_{162}$	−0.4	1.3	2.5	2.6
Fe_{309}	0.3	2.5	2.4	2.9
$Fe_{309}Cu_{252}$	−0.4	1.0	2.5	2.7

equivalent) has a negatively aligned moment. The results are summarized in Table II, where it can be seen that, for both $Fe_{147}Cu_{162}$ and $Fe_{309}Cu_{252}$, the average moment on the Fe atoms at the interface with Cu is considerably reduced from the bare cluster value and the mean moment on the core is small and of opposite sign to that of the interface.

In the experimental study, the lattice spacing determined by EXAFS was 3.58 ± 0.02 Å and the magnetic moment was found to be in the range 0.5–0.9 μ_B per atom. We base our theoretical prediction on the moments of the embedded 147 and 309 atom clusters. The values at $a=3.58$ Å can be read off from the plots in Fig. 7 and provide an estimate of 0.4–0.8 μ_B, which is in rather good agreement with the experimental results. The experimental lattice spacing is clearly in the low moment regime. The calculated pattern of individual moments at $a=3.58$ Å appears qualitatively very similar to the $a=3.50$ Å plots of Figs. 8(a) and 8(b). The average core and interface moments are −0.5 and 1.6 μ_B for $Fe_{147}Cu_{162}$, and −0.6 and 1.5 μ_B for $Fe_{309}Cu_{252}$, respectively.

Obviously there are a few caveats in comparing the results of the calculations with the experimental data. Our calculations are on core-shell particles rather than on embedded clusters. However it does appear that the sensitivity of the Fe moment to the number of Cu shells is rather weak. Thus it is unlikely that a true embedding will change the results much. Probably, more important, is the shape of the particle and the quality of the Fe/Cu interface. The spread in values of the experimental moments is likely to be a reflection of variations in particle shape and the degree of epitaxy at the particle-matrix interface. We have considered just high-symmetry clusters with perfect interface epitaxy and we obtain a moment distribution with the same symmetry as the cluster. Obviously deviations from these idealized configurations will change the results but we expect that the moments would still lie within a window of ~0.5 μ_B width somewhat below 1 μ_B.

Lattice relaxation could also be important. The calculations reported above were done with fixed lattice spacings. To test the sensitivity to lattice relaxation, we performed an *ab initio* calculation on a $Fe_{55}Cu_{92}$ cluster to find the ground state with optimized geometry. For fixed lattice spacings at or near $a=3.58$ Å, there are a number of metastable solutions. Two are close in energy: a high moment state with all spins aligned parallel and a low moment state. In the low moment state, all the spins are parallel except those that on the atoms that are nearest neighbor to the central one and these are antiparallel to the rest. The configurations of up and down spins are rather more complex for the larger particles as can be seen in Figs. 8(a) and 8(b). We found two other configurations of up and down spins for the $Fe_{55}Cu_{92}$ cluster, but in those cases the energies were considerably higher.

We performed a search for optimum geometries starting with the lattice spacing at $a=3.58$ Å for both the high and low spin starting configurations. We were unable to obtain convergence to a new geometry with the high spin initialization but, with the low spin start, convergence to a lower-energy geometry occurred very easily. There was just a small increase (by 6%) in the moment from its unrelaxed value of ~1.5 μ_B. The relaxation resulted in a range (2.46–2.56 Å) of nearest-neighbor distances between Fe atoms in the cluster core, the smallest being between the central atom and its neighbors. The average first and second neighbor Fe–Fe distances were 2.53 and 3.58 Å, respectively. The rather good agreement with the experimental values at low volume filling fraction is rather striking but not overly significant since the $Fe_{55}Cu_{92}$ cluster is small compared to the experimental Fe particles and is covered with just a single Cu shell. However, the calculation can be taken as an indication that geometry optimization tends to further stabilize the low spin configuration.

Finally, we note that we performed a number of calculations of the orbital moment for representative systems ($Fe_{55}Cu_{92}$, $Fe_{55}Cu_{254}$, $Fe_{147}Cu_{162}$) and lattice spacings. The calculations show that the orbital moments are small compared to the spin moments. The range of values obtained was: 3.40 Å (0.016–0.020 μ_B per atom), 3.65 Å (0.065–0.12 μ_B per atom), and 3.70 Å (0.10–0.14 μ_B per atom). Clusters with lower symmetry than the ones studied here are quite likely to show an orbital moment somewhat larger than these values, but even so it would be surprising if the orbital moment was above 10% of the spin moment.

V. CONCLUSIONS

This paper reports the results of a combined experimental and theoretical study of Fe nanoclusters of a mean size of ~260 atoms embedded in a Cu matrix. There is considerable interest in the behavior of fcc Fe precipitates in Cu. However in this study involving well-defined particles, a direct cluster deposition technique was used to prepare the embedded Fe nanoclusters. For a VFF of less than the three-dimensional percolation threshold, our measurements show that the Fe clusters have an fcc structure with a lattice parameter of 3.58 ± 0.02 Å and exhibit a net magnetic moment of 0.4–0.9 μ_B per atom. A transition to the higher spin bulk value is observed accompanying a transition from the fcc to bcc structure as the VFF crosses the percolation threshold.

The theoretical calculations, which used *ab initio* and tight-binding techniques, were done on Fe particle/Cu shell clusters and explored the magnetism of the Fe particles as a function of lattice spacing and Cu shell thickness. The effect of geometry relaxation was also investigated, and the contribution of the orbital moment was found to be very small (less than 10%). A picture emerges of configurations of up and down spin Fe local moments, giving a net moment for the particles of 0.4–0.8 μ_B per atom, which is consistent

with the experimental observations. The moments on those Fe atoms that interface with the Cu coating mostly (but not all) align parallel with each other giving an average moment at the interface of about 1.5 μ_B per atom. There is greater cancellation between up and down spins on atoms in the Fe core (noninterface Fe atoms) and for these the average moment is about −0.5 μ_B per atom. For larger clusters, one can expect a decrease in the net moment, since the proportion of atoms that are at the interface will decrease and the cancellation between up and down spins on the core atoms will become more complete. To a first approximation, of course, the net moment on a cluster is determined by the number of uncompensated spins (difference in numbers of up and down spins). However there is considerable variation in the magnitude of individual moments so writing the net moment of the cluster simply as the product of the magnitude of a moment and the number of uncompensated spins would be overly naive.

ACKNOWLEDGMENTS

The authors are grateful to S. Fiddy for his assistance. This work was supported by the EC project NANOSPIN (Contract No. NMP4-CT-2004–13545).

*Present address: Department of Chemistry, University of Manitoba, Winnipeg R3T 2N2, Canada.

[1] I. M. L. Billas, J. A. Becker, A. Châtelain, and W. A. de Heer, Phys. Rev. Lett. **71**, 4067 (1993).
[2] S. H. Baker, C. Binns, K. W. Edmonds, M. J. Maher, S. C. Thornton, S. Louch, and S. S. Dhesi, J. Magn. Magn. Mater. **247**, 19 (2002).
[3] J. T. Lau, A. Fohlisch, R. Nietubyc, M. Reif, and W. Wurth, Phys. Rev. Lett. **89**, 057201 (2002).
[4] A. Perez, P. Melinon, V. Dupuis, P. Jensen, B. Prevel, J. Tuiallon, L. Bardotti, C. Martet, M. Treilleux, M. Broyer, M. Pellarin, J. L. Vaille, B. Palpant, and J. Lerme, J. Phys. D **30**, 709 (1997).
[5] C. Binns, K. N. Trohidou, J. Bansmann, S. H. Baker, J. A. Blackman, J. P. Bucher, D. Kechrakos, A. Kleibert, S. Louch, K. H. Meiwes-Broer, G. M. Pastor, A. Perez, and Y. Xie, J. Phys. D **38**, R357 (2005).
[6] S. H. Baker, M. Roy, S. Louch, and C. Binns, J. Phys.: Condens. Matter **18**, 2385 (2006).
[7] A. T. Paxton, M. Methfessel, and H. M. Polatoglou, Phys. Rev. B **41**, 8127 (1990).
[8] G. Y. Guo and H. H. Wang, Chin. J. Physiol. **38**, 949 (2000).
[9] S. C. Abrahams, L. Guttman, and J. S. Kasper, Phys. Rev. **127**, 2052 (1962).
[10] G. J. Johanson, M. B. McGirr, and D. A. Wheeler, Phys. Rev. B **1**, 3208 (1970).
[11] Y. Tsunoda, S. Imada, and N. Kunitomi, J. Phys. F: Met. Phys. **18**, 1421 (1988).
[12] K. Haneda, Z. X. Zhou, A. H. Morrish, T. Majima, and T. Miyahara, Phys. Rev. B **46**, 13832 (1992).
[13] O. K. Andersen, J. Madsen, U. K. Poulsen, O. Jepsen, and J. Kollar, Physica B (Amsterdam) **86-88**, 249 (1977).
[14] J. Kübler, Phys. Lett. **81A**, 81 (1981).
[15] D. Bagayoko and J. Callaway, Phys. Rev. B **28**, 5419 (1983).
[16] V. L. Moruzzi, P. M. Marcus, K. Schwarz, and P. Mohn, Phys. Rev. B **34** 1784 (1986).
[17] V. L. Moruzzi, P. M. Marcus, and J. Kübler, Phys. Rev. B **39**, 6957 (1989).
[18] G. L. Krasko, Phys. Rev. B **36**, 8565 (1987).
[19] D. Guenzburger and D. E. Ellis, Phys. Rev. B **51**, 12519 (1995).
[20] Y.-M. Zhou, W.-Q. Zhang, L.-P. Zhong, and D.-S. Weng, J. Magn. Magn. Mater. **145**, L273 (1995).
[21] Y.-M. Zhou, W.-Q. Zhang, L.-P. Zhong, and D.-S. Weng, J. Magn. Magn. Mater. **167**, 136 (1997).
[22] L. T. Kong and B. X. Liu, Appl. Phys. Lett. **84**, 3627 (2004).
[23] L. T. Kong and B. X. Liu, J. Alloys Compd. **414**, 36 (2006).
[24] O. K. Andersen and O. Jepsen, Phys. Rev. Lett. **53**, 2571 (1984).
[25] O. K. Andersen, Z. Pawlowska, and O. Jepsen, Phys. Rev. B **34**, 5253 (1986).
[26] H. J. Nowak, O. K. Andersen, T. Fujiwara, O. Jepsen, and P. Vargas, Phys. Rev. B **44**, 3577 (1991).
[27] H. Magnan, D. Chandesris, B. Villette, O. Heckmann, and J. Lecante, Phys. Rev. Lett. **67**, 859 (1991).
[28] S. Müller, P. Bayer, C. Reischl, K. Heinz, B. Feldmann, H. Zillgen, and M. Wuttig, Phys. Rev. Lett. **74**, 765 (1995).
[29] R. D. Ellerbrock, A. Fuest, A. Schatz, W. Keune, and R. A. Brand, Phys. Rev. Lett. **74**, 3053 (1995).
[30] D. Schmitz, C. Charton, A. Scholl, C. Carbone, and W. Eberhardt, Phys. Rev. B **59**, 4327 (1999).
[31] J. Shen, M. Klaua, P. Ohresser, H. Jenniches, J. Barthel, Ch. V. Mohan, and J. Kirschner, Phys. Rev. B **56**, 11134 (1997).
[32] J. Shen, P. Ohresser, Ch. V. Mohan, M. Klaua, J. Barthel, and J. Kirschner, Phys. Rev. Lett. **80**, 1980 (1998).
[33] U. Gradmann and H. O. Isbert, J. Magn. Magn. Mater. **15-18**, 1109 (1980).
[34] M. A. Torija, Z. Gai, N. Myoung, E. W. Plummer, and J. Shen, Phys. Rev. Lett. **95**, 027201 (2005).
[35] P. Gorria, D. Martínez-Blanco, J. A. Blanco, A. Hernando, J. S. Garitaonandia, L. Fernandez Barquin, J. Campo, and R. I. Smith, Phys. Rev. B **69**, 214421 (2004).
[36] P. Gorria, D. Martínez-Blanco, J. A. Blanco, M. J. Pérez, A. Hernando, L. Fernandez Barquin, and R. I. Smith, Phys. Rev. B **72**, 014401 (2005).
[37] A. Orecchini, F. Sacchetti, C. Petrillo, P. Postorino, A. Congeduti, C. Giorgetti, F. Baudelet, and G. Mazzone, J. Alloys Compd. **424**, 27 (2006).
[38] S. Khmelevskyi and P. Mohn, Phys. Rev. B **71**, 144423 (2005).
[39] S. H. Baker, S. C. Thornton, K. W. Edmonds, M. J. Maher, C. Norris, and C. Binns, Rev. Sci. Instrum. **71**, 3178 (2000).
[40] N. Binsted, EXCURV98: Daresbury Laboratory Computer Program, 1998.
[41] D. Stauffer and A. Aharony, *Introduction to Percolation Theory* (Taylor and Francis, London, 1994).
[42] S. J. Gurman and J. B. Hendry, Solid State Commun. **20**, 287 (1976).
[43] D. R. Jennison, P. A. Schultz, and M. P. Sears, J. Chem. Phys. **106**, 1856 (1997).

[44] V. Kumar and Y. Kawazoe, Phys. Rev. B **66**, 144413 (2002).
[45] P. Nava, M. Sierka, and R. Ahlrichs, Phys. Chem. Chem. Phys. **5**, 3372 (2003).
[46] M. L. Tiago, Y. Zhou, M. M. G. Alemany, Y. Saad, and J. R. Chelikowsky, Phys. Rev. Lett. **97**, 147201 (2006).
[47] G. Rollmann, M. E. Gruner, A. Hucht, R. Meyer, P. Entel, M. L. Tiago, and J. R. Chelikowsky, Phys. Rev. Lett. **99**, 083402 (2007).
[48] B. Delley, J. Chem. Phys. **92**, 508 (1990).
[49] J. P. Perdew, in *Electronic Structure of Solids, '91*, edited by P. Ziesche and H. Eschrig (Akademie, Berlin, 1991).
[50] J. P. Perdew, J. A. Chevary, S. H. Vosko, K. A. Jackson, M. R. Pederson, D. J. Singh, and C. Fiolhais, Phys. Rev. B **46**, 6671 (1992).
[51] J. P. Perdew, K. Burke, and Y. Wang, Phys. Rev. B **54**, 16533 (1996).
[52] W. Harrison, *Electronic Structure and the Properties of Solids* (Freeman, San Francisco, 1980).
[53] A. N. Andriotis and M. Menon, Phys. Rev. B **57**, 10069 (1998).
[54] Y. Xie and J. A. Blackman, Phys. Rev. B **64**, 195115 (2001).
[55] Y. Xie and J. A. Blackman, Phys. Rev. B **66**, 085410 (2002).
[56] Y. Xie and J. A. Blackman, Phys. Rev. B **66**, 155417 (2002).
[57] Y. Xie and J. A. Blackman, J. Phys.: Condens. Matter **16**, 8589 (2004).
[58] Y. Xie and J. A. Blackman, Phys. Rev. B **74**, 054401 (2006).
[59] Y. Xie and J. A. Blackman, Phys. Rev. B **73**, 214436 (2006).
[60] P. Bruno, in *Magnetismus von Festkörpern und Grenzflächen*, IFF-Ferienkurs, edited by P. H. Dederichs, P. Grünberg, and W. Zinn (Forschungszentrum Jülich, Germany, 1993), pp. 24.1–24.27.